Approaching the perfect diode limit through a nonlinear interface

Alexandre A. A. Almeida[1], Lucianno Defaveri[2], and Celia Anteneodo[1,3]
[1]Department of Physics, PUC-Rio, Rio de Janeiro, 22453-900 RJ, Brazil
[2]Department of Physics, Bar Ilan University, Ramat-Gan 52900, Israel and
[3]Institute of Science and Technology for Complex Systems, INCT-CS, Rio de Janeiro, Brazil

We consider a system formed by two different segments of particles, coupled to two thermal baths, one at each end, modeled by Langevin thermostats. The particles in each segment interact harmonically and are subject to an on-site potential, for which, three different types are considered, namely, harmonic, ϕ^4, and Frenkel-Kontorova. The two segments are nonlinearly coupled, according to a power-law potential between interfacial particles, characterized by the exponent μ and strength k_μ. Thermal rectification is investigated by integrating the equations of motion and computing the heat fluxes. From a systematic study, varying the interface parameters μ, characteristic length ℓ, and k_μ, the average temperature T_m and relative difference of end temperatures $\Delta_{rel} \equiv \Delta T/T_m$, we discuss the conditions under which optimal rectification is achieved. At high temperatures, rectification is optimal at a finite μ. When the average temperature is sufficiently low, maximal rectification (close to 100%) is achieved in the infinite-square-well limit of the interface potential ($\mu \to \infty$).

I. INTRODUCTION

A thermal diode is a material whose thermal conductivity along a given axis changes depending on the direction of the heat flux. Pioneering works have theoretically shown the possibility of this effect [1, 2]. Soon after, a first experimental evidence of the diode effect appeared [3]. Since then, much work has focused on finding the conditions to improve the diode efficiency both theoretically [4–6] and experimentally [7–12].

Nonlinearity and asymmetry are required to break the symmetry of inversion in flux direction (see for instance refs. [13–15]). Asymmetry can be achieved in several ways, for instance, by mass-graded chains [6, 16], homogeneous chains with asymmetric interactions [17], simply by the presence of impurities or defects [18, 19], or coupling two or more different segments [1]. Interactions between particles or with the substrate must be anharmonic to yield temperature dependence of the conductivity [13].

Particularly the interface between segments plays a crucial role [13, 18, 20–23], since it can affect the overlap of the phonon bands of the each segment, which selects the conducting modes. In the case of two segments, the phonon bands of each decoupled segment are different due to the asymmetry or distinct characteristics of each segment, and the nonlinear interactions make the spectra temperature-dependent. Then, the band overlap can change under flux inversion, giving rise to a preferential direction for heat conduction. If the coupling is weak and linear, we expect that similar overlaps to those obtained for isolated segments will hold for the coupled chain. As the communication between segments (controlled by the interfacial stiffness) increases, band overlap will be affected, and differences related to temperature inversion blurred [1], reducing rectification. However, if the coupling were nonlinear, band overlap might become more complex [24], with strong interference of bands even for weak coupling strength, and efficiency optimization may appear under certain nontrivial conditions.

In this context, we address the following questions. Which is the effect of a nonlinear interface in two-segment systems subject to thermal baths at the ends? Under which conditions can this nonlinearity improve the performance of the thermal diode? To find insights about the answers to these questions, we consider two segment-chains of particles that are harmonically coupled and subject to on-site potentials (either harmonic, ϕ^4 or Frenkel-Kontorova), while the segments are coupled through a power-law potential V_μ, with exponent μ, between interfacial particles. Additionally, we consider Langevin baths connected at the ends, and fixed boundary conditions. A schematic representation of the studied family of systems is given in Fig. 1.

From the integration of the equations of motion, we obtain the heat currents and a quantifier of rectification,

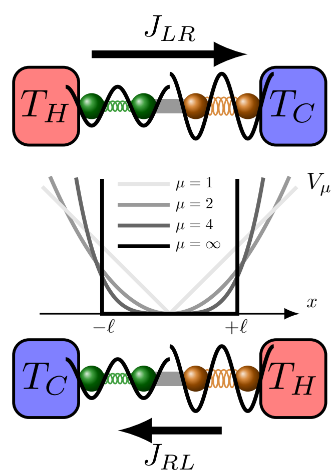

FIG. 1: Schematic representation of the system formed by two different segments nonlinearly coupled and subject to thermal baths at the ends, producing rectification under flux inversion.

and explore the effects of the nonlinear junction. The paper is organized as follows. We define the model in Sec. II and the methods in Sec. III. Results of numerical simulations for the system formed by harmonic segments joined by a nonlinear interface, and a discussion of the perfect-diode limit, are presented in Sec. IV. In Sec. V, we study systematically the dependence of the rectification factor on the model parameters, for momentum non-conserving segments. A discussion and concluding remarks are presented in Sec. VI.

II. MATHEMATICAL MODEL

In each of two, left (L) and right (R), segments, particles of identical mass m interact harmonically with their first neighbors, with stiffness constant $k_{L/R}$, and are subject to an on-site potential $V_{L/R}$, representing the interaction with a substrate of negligible thermal conductivity. The two segments are coupled through a power-law potential. Namely, the full system is governed by the Hamiltonian

$$\begin{aligned}\mathcal{H} &= \sum_{n=1}^{N}\frac{1}{2}\frac{p_n^2}{m}+\sum_{n=1}^{M}\frac{k_L}{2}(x_n-x_{n-1}-a)^2+\sum_{n=1}^{M}V_L(x_n)\\ &\quad + V_\mu(x_M-x_{M+1})\\ &\quad + \sum_{n>M}^{N}\frac{k_R}{2}(x_{n+1}-x_n-a)^2+\sum_{n>M}^{N}V_R(x_n), \end{aligned} \tag{1}$$

where x_n (with $n=1,\ldots,N=2M$, indexed from left to right) is the coordinate of particle n, p_n its momentum, a is the lattice constant, and $k_{L/R}$ are stiffness constants. As on-site potentials $V_{R/L}$, we will consider diverse cases defined below. Moreover, boundary conditions remain fixed, such that $x_{N+1}=x_0=0$, at all time. The end particles 1 and N, are immersed in thermal baths represented by Langevin thermostats, at temperatures T_L and T_R. Then, the equations of motion are given by

$$\dot p_1 = m\ddot x_1 = -\frac{\partial\mathcal{H}}{\partial x_1}-\gamma\dot x_1+\eta_1(t), \tag{2}$$

$$\dot p_n = m\ddot x_n = -\frac{\partial\mathcal{H}}{\partial x_n}\quad \text{for } n=2\ldots N-1, \tag{3}$$

$$\dot p_N = m\ddot x_N = -\frac{\partial\mathcal{H}}{\partial x_N}-\gamma\dot x_N+\eta_N(t), \tag{4}$$

where η_1 and η_N are uncorrelated stochastic Gaussian white noises with zero mean and

$$\begin{aligned}\langle\eta_1(t)\eta_1(t')\rangle &= 2\gamma k_B T_L\,\delta(t-t'),\\ \langle\eta_N(t)\eta_N(t')\rangle &= 2\gamma k_B T_R\,\delta(t-t').\end{aligned} \tag{5}$$

Finally, in order to study the impact of the nonlinearity of the interfacial interaction, we consider that

$$V_\mu(x)=\frac{k_\mu}{\mu}\left(\frac{|x|}{\ell}\right)^\mu \tag{6}$$

where k_μ is a positive constant, ℓ is the characteristic length of the interaction and the exponent is $\mu\geq 1$. Even though ℓ could be absorbed into k_μ, we keep track of both parameters separately so that in the limit $\mu\to\infty$, which is equivalent to an infinite square well, we can control the size of the well through ℓ. The force derived from this interaction includes two classes of nonlinearities: for $\mu>2$ ($\mu<2$) the force is super(sub)-linear as a function of the displacement from the equilibrium position. V_μ ranges from the triangular ($\mu=1$) to the infinite square well ($\mu\to\infty$) potentials, and include the harmonic and quartic ones. The exponent $\mu\neq 2$, not necessarily integer, gives rise to oscillations beyond the simple harmonic case, associated to nonlinear responses [25–28].

For the on-site potential, we analyze different cases, starting with the harmonic pinning given by

$$V(x_n)=\frac{A}{2}\left(x_n-na\right)^2. \tag{7}$$

In such case, the Fourier law does not hold, a flat bulk temperature profile and conductivity that scales with N is known to occur due to momentum conservation [29–31].

As substrates that break momentum-conservation and allow Fourier-law, we consider the following ones.

(i) A particular case of the ϕ^4 potential, namely

$$V(x_n)=\frac{A}{4}\left(x_n-na\right)^4, \tag{8}$$

where A is a positive constant. This unbounded potential has been thoroughly studied in the literature of thermal conduction [31–36].

(ii) The second case is a paradigm of periodic bounded potential, the Frenkel-Kontorova (FK) potential [37, 38], with period a, given by

$$V(x_n)=\frac{A}{2\pi}\left[1-\cos\left(2\pi x_n/a\right)\right]. \tag{9}$$

This model has also been studied as paradigm of normal heat transport [33, 34, 38–40].

III. METHODS

The equations of motion (2)-(4) were numerically integrated by means of an adaptive Euler-Maruyama method, with maximum time step $\Delta t=10^{-4}$ or stochastic higher-order Runge-Kutta method with time step $\Delta t=10^{-3}$ [41]. Typically, the total simulation time is $t_{max}=10^5$, and the transient time $t_{trans}=10^3$. In all cases, each (R/L) segment was characterized by values of the force amplitudes with the relation $A_R/A_L=5$, and $k_R/k_L=5$, in order to produce significant asymmetry. That is, without loss of generality, the right-side potential was chosen to have larger amplitude than the left-side one. In numerical experiments, we set $A_L=k_L=1$, except in the FK case where we used $k_L=0.2$. Moreover, we set $m = a = \gamma = 1$ and worked with small sizes $N = 2$ and 4. For simplicity, we set $k_B = 1$ and treat temperature in energy units.

In the extreme $\mu \to \infty$, the interface potential given by Eq. (6), tends to an infinite square well, null for $x \in [-\ell, \ell]$, infinite otherwise. For numerical integration of two-particle systems, we changed variables to the center of mass cordinate R and the relative coordinate r between interfacial particles, ruled by free motion inside the well with reflecting boundaries at $\pm\ell$.

We measured the long-time value of the heat current

$$J \;=\; \left\langle V'_\mu(x_M - x_{M+1}) \left(\frac{\dot{x}_M + \dot{x}_{M+1}}{2} \right) \right\rangle \qquad (10)$$

averaged over time and over realizations, typically $\mathcal{N} = 10^3$ samples, unless differently specified.

As measure of rectification, we considered the coefficient

$$R = \frac{|J_{LR} - J_{RL}|}{|J_m|}\,, \qquad (11)$$

where J_{LR} and J_{RL} are the absolute values of the currents in each direction (obtained by inverting the heat baths), and $J_m = (J_{LR} + J_{RL})/2$. Depending on the on-site and interface potentials, either J_{LR} or J_{RL} turns out to be the largest one [13].

Temperatures were characterized by the average $T_m = (T_L + T_R)/2$, and the relative temperature difference, $\Delta_{rel} = (T_L - T_R)/T_m$, hence $T_{L/R} = T_m(1 \pm \Delta_{rel}/2)$, and $|\Delta_{rel}| \le 2$.

IV. HARMONIC ON-SITE POTENTIAL

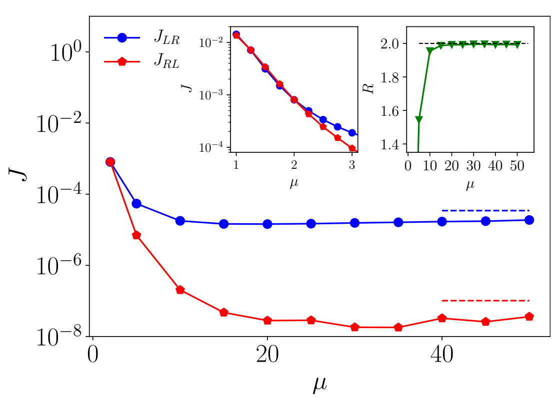

FIG. 2: Currents J_{LR} and J_{RL} as a function of the interfacial exponent μ, for a harmonic system with two particles ($N = 2$). The left inset is a zoom around $\mu = 2$ (fully harmonic system). The right-side inset shows the rectification factor R vs μ. For comparison, we indicate by dashed lines values in the limit $\mu \to \infty$ studied in Section IV A. We used $k_\mu = 0.5$, $\ell = 1$, $T_m = 0.05$ and $\Delta_{rel} = 1$, and $\mathcal{N} = 10^4$ samples were used to compute the average currents.

The heat fluxes as a function of μ, at low average temperature T_m, are shown in Fig. 2. The dominant current changes at $\mu = 2$, where the system becomes fully harmonic and both currents coincide. The currents decrease with μ, tending to a finite value, such that the rectification coefficient $R = |\Delta J/J_m|$ approaches a level which is close to the perfect diode one ($R = 2$), for the chosen parameter values given in the caption. This indicates that the more confining the potential, the stronger the diode effect, although both currents decrease in intensity.

This result suggests to study the limiting case of the infinite-square well potential.

A. Infinite-square-well interface

For the infinite square well of half-width ℓ obtained in the limit $\mu \to \infty$ of Eq. (6), we show in Fig. 3 the effect of the width ℓ on the currents and rectification factor (remaining parameters have the same values used in Fig. 2). Energy transfer occurs only through collisions with the walls (that we call stretches), that is when the relative displacement reaches $r = \pm\ell$. The rate ρ at which r reaches a wall always decays with ℓ and increases with T_m. We can extract further insights from the expression for the variance of r when the system has no walls, that is, $\langle r^2 \rangle = T_L/A_L + T_R/A_R \sim \ell^2$, which increases with ℓ and is clearly asymmetric upon exchanging temperatures, and therefore, the number of collisions is also asymmetric. This effect is clearly visible in Fig. 3, where we plot histograms of $\rho\Delta T$, where ρ is the count of stretches per unit time. When $\ell \to 0$, the relative coordinate tends to be confined near zero, therefore, fluctuations, and hence the asymmetry, are suppressed. In this limit, the dominant motion is that of the center of mass, and the currents in each direction coincide. In the limit of large ℓ, and low enough temperature, a maximal efficiency close to $R = 2$

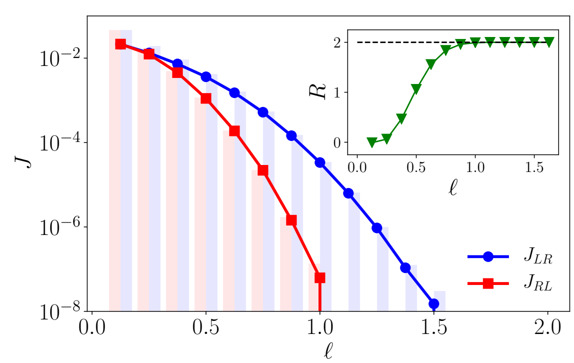

FIG. 3: Currents for a harmonic system with two particles ($N = 2$) as a function of the width ℓ of the **infinite-square-well interface**. The inset shows the rectification factor and the dashed horizontal line refers to the **perfect diode** effect, nearly attained for $\ell \gtrsim 1$. The histogram of $\rho\Delta T$, where ρ is the the number of stretches per unit time, is also shown in the main plot. $T_m = 0.05$ and $\Delta_{rel} = 1$.

(perfect diode) is is attained when $\mu \to \infty$. For instance, in the case of the figure, $\ell = 1$ is enough to achieve the perfect diode within 0.5% tolerance ($R = 1.992$).

Let us also inspect the current J as a function of ΔT_{rel}, presented in Fig. 4, for $T_m = 0.05$ and $\ell = 1$. The diode effect is enhanced for increasing $|\Delta_{rel}|$. Notice that the current coincides with $\rho \Delta T$. For negative ΔT, the flux is very small but not vanishing, although a null count of stretches can occur due to the limited observation time window. Notice that, for $\Delta_{rel} = 1$, the currents correspond to the limiting values (dashed segments) in Fig. 2.

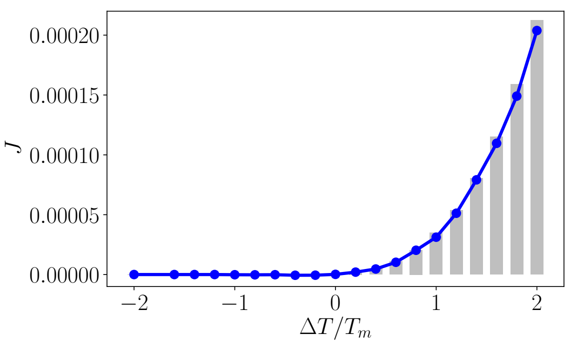

FIG. 4: Heat flux vs. $\Delta_{rel} \equiv \Delta T/T_m$ (blue symbols) for the harmonic system with **infinite-square-well interface**. The gray bars represent $\rho \Delta T$, where ρ is the rate of stretches. $N = 2$, $\ell = 1$ and $T_m = 0.05$.

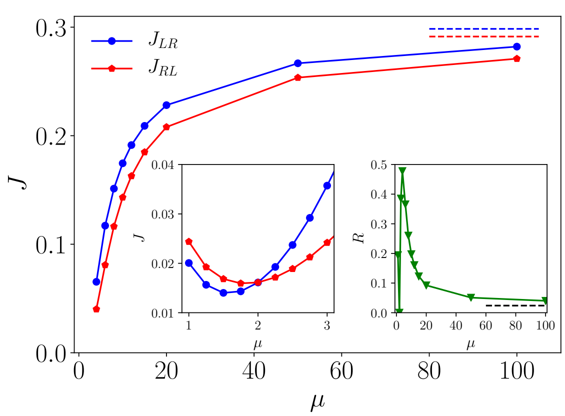

FIG. 5: Currents J_{LR} and J_{RL} vs. μ, for a harmonic system with two particles ($N = 2$). The left inset shows the behavior around $\mu = 2$ (fully harmonic system). The right-side inset shows the rectification factor R vs μ. The maximal R occurs near above $\mu = 4$ and R tends to low level for large μ. We used $k_\mu = 0.5$, $\ell = 1$ and $T_m = \Delta_{rel} = 1$.

B. More about finite μ

Let us now discuss the behavior of the system at large temperature T_m. The currents and rectification factor as a function of μ are presented in Fig. 5. Differently to the case of Fig. 2, the currents are large but of the same order of magnitude, hence the rectification effect is weak. The currents coincide when $\mu = 2$, occurring inversion of the preferential direction, and R is maximal at $\mu \gtrsim 4$.

In Fig. 6, we show plots of R vs. μ, varying also T_m (a), Δ_{rel} (b) and k_μ (c), using in this case $N = 4$. In all cases, $R(\mu = 2) = 0$, unless finite size fluctuations, which become significant when currents are very small, as happens for low temperature difference Δ_{rel}, or weak interactions (small k_μ).

Notice, in Fig. 6(a), how the behavior of R vs μ changes with the temperature T_m. At at low T_m, the rectification increases with μ, but for large temperatures, has a maximum at finite μ, as also observed for $N = 2$ in Figs. 2

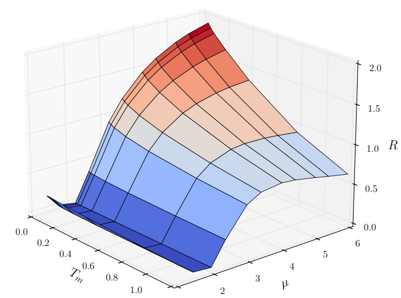

(a)

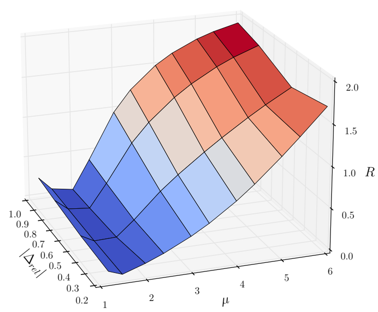

(b)

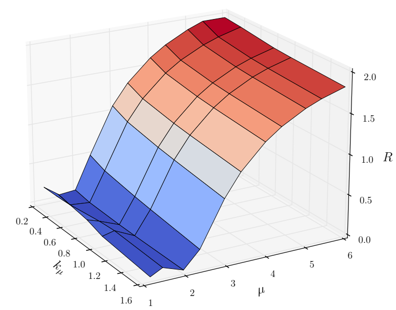

(c)

FIG. 6: **On-site harmonic potential**. Rectification factor R as a function of the exponent μ, varying also (a) the average temperature T_m, with $k_\mu = 0.5$ and $\Delta_{rel} = 1$. (b) the relative difference Δ_{rel} with $T_m = 0.05$ and $k_\mu = 0.5$, and (c) the coefficient k_μ, with $T_m = 0.05$, $\Delta_{rel} = 1$ and $N = 4$.

and 5, respectively. The cuts of the 3D plot (a) for fixed T_m are shown in the Appendix.

For fixed μ, R decays mononotically with T_m. Increasing Δ_{rel}, with $T_m = 0.05$ and $k_\mu = 0.5$, has no qualitative impact, out of reinforcing rectification as seen in Fig. 6(b), and also in Fig.fig:infinite-dT for the infinite-μ limit of the two-particle system.

Regarding the dependence on k_μ (c), cuts of the surface of R at fixed μ indicate that R decays with k_μ. For small k_μ, both currents J_{LR} and J_{RL} increase as k_μ^2, but as the stiffness coefficient increases, both currents approach each other, hence R decays. This effect observed also for the other on-site potentials studied is illustrated in the Appendix. The scaling $J \sim k_\mu^2$ has been also observed in Fig. 6(c) for a linear interface [1, 13]). Notice that increasing k_μ is related to decreasing the characteristic size ℓ, according to Eq. (6).

In sum, for harmonic pinning, the diode efficiency increases with μ for low T_m, and this effect is strengthened with increasing ΔT_{rel} and small values of k_μ, allowing the rectification to approach the maximal value $R = 2$ within a desired precision. However, at high temperatures, the diode effect is weaker and R is optimal at finite μ.

In the next section, we show results for momentum non-conserving systems, subject to ϕ^4 or FK on-site potentials, which follow Fourier's law. Although some new features emerge, the main points highlighted up to know still hold.

V. MOMENTUM NON-CONSERVING ON-SITE POTENTIALS

A. ϕ^4 on-site potential

3D plots of the rectification R, vs. μ together with T_m, $|\Delta_{rel}|$, or k_μ, are displayed in Fig. 7, for systems with $N = 4$ subject to the ϕ^4 on-site potential.

In Fig. 7(a), we can see that the dependency of R with (μ, T_m) presents a saddle point not observed in the harmonic case. First, the full system is not purely harmonic when $\mu = 2$ due to the ϕ^4 pinning, therefore $R(\mu = 2) > 0$. Moreover, in contrast to the monotonic behavior of the harmonic system with T_m, there is an optimal temperature T_m for rectification. But, similarly to the harmonic chain, we observe that R increases with μ for low temperatures and there is a finite optimal μ for high temperatures.

In Fig. 7(b), for $T_m = 1$, we note that the rectification factor R increases with $|\Delta_{rel}|$ and the optimal μ is shifted to larger values. In Fig. 7(c), we note the reduction of rectification with increasing k_μ, and the enhanced rectification with increasing μ at weak coupling, while, for stronger coupling, rectification occurs at finite μ near the harmonic value.

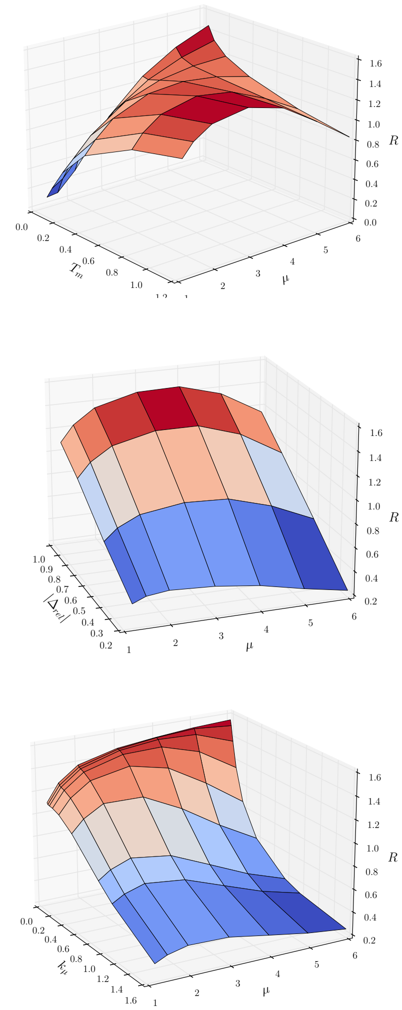

(a) (b) (c)

FIG. 7: **On-site ϕ^4 potential**. Rectification factor R as a function of the exponent μ, varying also (a) the average temperature T_m, with $k_\mu = 0.2$ and $\Delta_{rel} = 1$, (b) the relative difference Δ_{rel} with $T_m = 1.0$ and $k_\mu = 0.1$, and (c) the coefficient k_μ, with $T_m = \Delta_{rel} = 1$ and $N = 4$.

B. Frenkel-Kontorova on-site potential

In numerical experiments of systems with FK pinning, we used $N = 4$ particles, and $k_L = 0.2$. In Fig. 8, at first sight, we observe that $\mu < 2$, can produce enhanced rectification, at low T_m. Similar behavior was observed in the harmonic case in Fig. 5. In fact, at low T_m, particles subject to the FK on-site potential dwell in a nearly harmonic well. If additionally the interfacial potential is harmonic ($\mu = 2$), then the diode effect is spoiled. Differently to the previous potentials studied, which are unbounded, the profile of the FK potential becomes irrelevant for very large temperatures and the surface of R flattens. Furthermore, at very high temperatures, when the thermal energy k_BT becomes of the same order of a threshold energy $A/(2\pi)$, the particles leave their wells and start occupying other ones, giving rise to a transition in the behavior of the transport coefficients [38–40]. In the present study we avoided these regimes that are beyond our present focus.

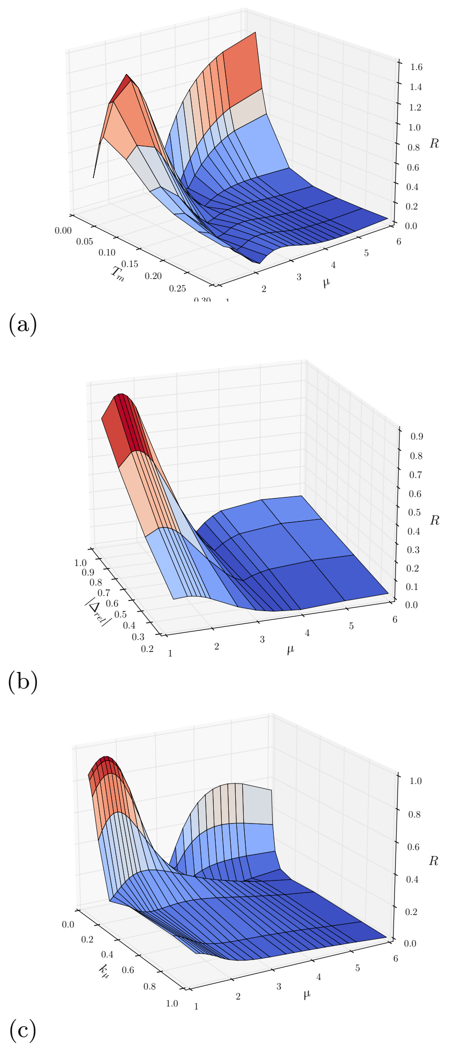

FIG. 8: **On-site FK potential**. Rectification factor R as a function of the exponent μ, varying also (a) the average temperature T_m, with $k_\mu = 0.05$ and $\Delta_{rel} = 1$, (b) the relative difference Δ_{rel} with $T_m = 0.1$ and $k_\mu = 0.05$, and (c) the coefficient k_μ, with $T_m = 0.1$, $\Delta_{rel} = 1$ and $N = 4$.

The points where R vanishes, meaning that $J_{LR} = J_{RL}$, indicate the inversion of the preferential direction. The inversion point can be shifted depending on the model parameters. Inversion was not observed for the ϕ^4 and harmonic potentials, above $\mu = 2$, but can occur below that value.

Beyond the features peculiar of the FK potential, we want to emphasize that, again in this case, when μ overcomes the inversion point, R increases with μ if T_m is low enough, namely, $T_m < 0.1$ in the case of Fig. 8(a), while decays with μ for large temperature.

VI. CONCLUSIONS

We considered segments that interact with a nonlinear force between interfacial particles, derived from the power-law potential $V_\mu(x) = \frac{k_\mu}{\mu}\left(\frac{|x|}{\ell}\right)^\mu$, which includes the infinite square well as a limiting case. Langevin thermal baths are connected to end particles.

For harmonic segments, the only nonlinearity is due to the interface. At low temperatures, we observed that thermal rectification is enhanced with increasing μ and the perfect-diode effect can be approached when $\mu \to \infty$, within a desired accuracy, at low k_μ, lowering T_m, and increasing Δ_{rel}. At high temperatures, the diode effect is weaker, and the optimal rectification is attained at a finite value of μ that depends on the other system parameters.

These effects have been observed not only for the harmonic segments but also for ϕ^4 and FK pinned ones. Moreover, the inversion of the preferential direction can be induced by changing the exponent μ.

Even for harmonic segments, the interfacial nonlinearity is enough to produce temperature-dependency and allows to optimize rectification. We have shown results for small systems with $N = 2$ and $N = 4$, but, since the perfect-diode can be governed by the interaction at the interface, the main qualitative features are expected to persist for longer chains.

Acknowledgements: We acknowledge partial financial support from Brazilian agencies CAPES (code 001)). C.A. is also grateful for partial financial support obtained from CNPq (311435/2020-3), and FAPERJ (CNE E-26/201.109/2021).

[1] B. Li, L. Wang, G. Casati, *Thermal diode: Rectification of heat flux*, Phys. Rev. Lett. 93, 184301 (2004).

[2] M. Terraneo, M. Peyrard, G. Casatti, *Controlling the energy flow in nonlinear lattices: A model for a thermal rectifier*, Phys. Rev. Lett. 88, 4 (2002).

[3] C.W. Chang, D. Okawa, A. Majumdar, A. Zettl, *Solid-state thermal rectifier*, Science, 314(5802), 1121–1124 (2006).

[4] E. Pereira, R.R. Ávila, *Increasing thermal rectification: Effects of long-range interactions*, Phys. Rev. E, 88, 032139 (2013).

[5] S. Chen, E. Pereira, G. Casati, *Ingredients for an efficient thermal diode*, EPL 111(3), 30004 (2015).

[6] S. Chen, D. Donadio, G. Benenti, G. Casati, *Efficient thermal diode with ballistic spacer*, Phys. Rev. E, 97, 030101 (2018).

[7] W. Kobayashi, Y. Teraoka, I. Terasaki, *An oxide thermal rectifier*, Applied Physics Letters 95, 171905 (2009).

[8] H. Tian, D. Xie, Y. Yang, T. Ren, G. Zhang, Y. Wang, C. Zhou, P. Peng, L. Wang, L. Liu, *A novel solid-state thermal rectifier based on reduced graphene oxide*, Sci. Rep. 2, 523 (2012).

[9] M. J. Martínez-Pérez, A. Fornieri, F. Giazotto, *Rectification of electronic heat current by a hybrid thermal diode*, Nature Nanotechnology 10, 303 (2015).

[10] C. Tso, C. Y. Chao, *Solid-state thermal diode with shape memory alloys*, Int. J. of Heat and Mass Transfer 93, 605 (2016).

[11] R. Shrestha, Y. Luan, X. Luo, S. Shin, T. Zhang, P. Smith, W. Gong, M. Bockstaller, T. Luo, R. Chen, K. Hippalgaonkar, S. Shen, *Dual-mode solid-state thermal rectification*, Nature Comm. 11, 4346 (2020).

[12] M. Kasprzak, M. Sledzinska, K. Zaleski, I. Iatsunskyi, F. Alzina, S. Volz, C.M. Sotomayor Torres, B. Graczykowski, *High temperature silicon thermal diode and switch*, Nano Energy 78, 105261 (2020).

[13] L. Defaveri, C. Anteneodo, *Analytical results for a minimalist thermal diode*, Phys. Rev. E 104, 014106 (2021).

[14] M. A. Simón, A. Alaña, M. Pons, A. Ruiz-Garcia, and J. G. Muga. *Heat rectification with a minimal model of two harmonic oscillators*, Phys. Rev. E 103, 012134 (2021).

[15] E. Pereira *Requisite ingredients for thermal rectification* Phys. Rev. E 96, 012114 (2017).

[16] M. Romero-Bastida, J.O.M. Peña, J.M. López, *Thermal rectification in mass-graded next-nearest-neighbor Fermi-Pasta-Ulam lattices*, Phys. Rev. E 95, 032146 (2017).

[17] G. Benenti, G. Casati, C. Mejía-Monasterio, M. Peyrard in "Thermal Transport in Low Dimensions: From Statistical Physics to Nanoscale Heat Transfer",S. Lepri (editor), (Springer International Publishing, 2016).

[18] M. Pons, Y. Y. Cui, A. Ruschhaupt, M. A. Simón and J. G. Muga, *Local rectification of heat flux*, EPL 119 64001 (2017).

[19] T. J. Alexander, *High-heat-flux rectification due to a localized thermal diode*, Phys. Rev. E 101, 062122 (2020).

[20] J. Wang and Z. Zheng, *Heat conduction and reversed thermal diode: The interface effect*, Phys. Rev. E 81, 011114 (2010).

[21] B. Li, J. Lan, and L. Wang, *Interface thermal resistance between dissimilar anharmonic lattices*, Phys. Rev. Lett. 95, 104302 (2005).

[22] L. Zhang, P. Keblinski, J.-S. Wang, and B. Li. *Interfacial thermal transport in atomic junctions*, Phys. Rev. B 83, 064303 (2011).

[23] B. Hu, L. Yang, Y. Zhang., Phys. Rev. Lett. 97. 124302 (2006).

[24] S. Liu, J. Liu, P. Hanggi, C. Wu, and B. Li, *Triggering waves in nonlinear lattices: Quest for anharmonic phonons and corresponding mean-free paths*, Phys. Rev. B 90, 174304 (2014).

[25] E. H. Colombo , L. A. C. A. Defaveri, C. Anteneodo, Phys. Rev. E 100, 032118 (2019).

[26] A. Dhar, A. Kundu, S. N. Majumdar, S. Sabhapandit, and G. Schehr, Phys. Rev. E 99, 032132 (2019).

[27] [25] P. Schmelcher, Phys. Rev. E 98, 022222 (2018).

[28] J.-C. Meiners and S. R. Quake, Phys. Rev. Lett. 84, 5014 (2000).

[29] O. Narayan, S. Ramaswamy, Phys. Rev. Lett. 89, 200601 (2002).

[30] S. Lepri, R. Livi, A. Politi, Phys. Rep. 377, 1 (2003).

[31] A. Dhar, *Heat transport in low-dimensional systems*, Adv. in Physics 57, 457 (2008).

[32] K. Aoki, J. Lukkarinen, H. Spohn, *Energy transport in weakly anharmonic chains*, Journal of Statistical Physics 124, 1105 (2006).

[33] A. V. Savin, Gendelman, *Heat conduction in one- dimensional lattices with on-site potential*, Phys. Rev. E 67, 041205 (2003).

[34] B. Hu, B. Li, H. Zhao, *Heat conduction in one- dimensional nonintegrable systems*, Phys. Rev. E 61, 3828 (2000).

[35] R. Lefevere, A. Schenkel, *Normal heat conductivity in a strongly pinned chain of anharmonic oscillators*, JSTAT 2006, L02001 (2006).

[36] N. Li and B. Li, *Parameter-dependent thermal conductivity of one-dimensional ϕ^4 lattice*, Phys. Rev. E 76, 011108(2007).

[37] B. Hu, B. Li, H. Zhao, *Heat conduction in one-dimensional chains*, Phys. Rev. E 57, 2992 (1998).

[38] M.J. Gillan, *Transport in the Frenkel-Kontorova model. I. Diffusion and single-particle motion*, J. Phys. C 18, 4485 (1985).

[39] M.J. Gillan, R.W. Holloway, *Transport in the Frenkel-Kontorova model. II. The diffusion coefficient*, J. Phys. C 18, 4903 (1985).

[40] M.J. Gillan, R.W. Holloway, *Transport in the Frenkel-Kontorova model. III. Thermal conductivity*, J. Phys. C 18, 5705 (1985).

[41] J. Verner, *Explicit Runge-Kutta Methods with Estimates of the Local Truncation Error*, SIAM Journal on Numerical Analysis 15(4), 772-790 (1978).

Appendix A: Heat fluxes and rectification

In Fig. A, we display the cuts of the 3D plots in Fig. 6(a), for different values of T_m indicated in the legend. In all cases, $R(\mu = 2) = 0$. For low T_m a monotonic dependency with μ is observed, but a maximum occurs at finite μ for high temperatures.

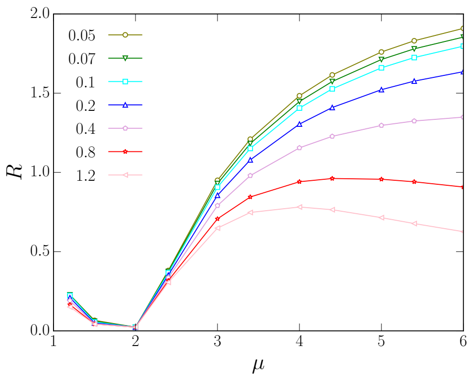

FIG. A1: Rectification R vs. μ for on-site harmonic potential, for different values of the average temperature T_m given in the legend. The other parameters are $N = 4$, $k_\mu = 0.5$ and $\Delta_{rel} = 1$.

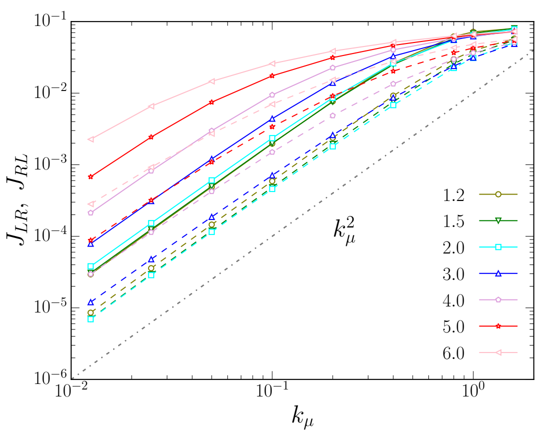

FIG. A2: Heat currents J_{LR} (full lines) and J_{RL} (dotted lines) vs. the stiffness k_μ for different values of μ indicated on the legend. The on-site potential is ϕ^4, $N = 4$, and $\Delta_{rel} = T_m = 1$. The straight dotted line, proportional to k_μ^2, is drawn for comparison.

The dependency of the heat currents with the interfacial coupling k_μ, for different values of μ is illustrated, in Fig. A2, for systems with ϕ^4 onsite potential, but the same scaling is observed for harmonic and FK potentials (not shown), with the observation that for FK the dominant current is $J_R L$.

The currents in the figure correspond to those that produced the values of R represented by the surface in Fig. 7(c). For weak coupling, the currents scale as k_μ^2, but for large k_μ the ratio of the currents decreases. This scaling, already known for the linear interface [1, 13], can be observed for any μ.

For systems with ϕ^4 pinning, we show in Fig. A3, the currents that produce the values of R of Fig. 7(a), exhibiting the effect of T_m, at moderate $k_\mu = 0.2$. For small temperature T_m, the currents decrease with μ, as also observed in the harmonic case of Fig. 2. However, notice the increase of the currents with μ for large T_m.

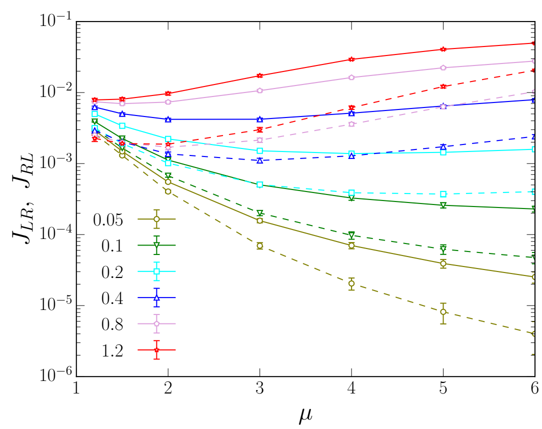

FIG. A3: Heat currents J_{LR} (full lines) and J_{RL} (dotted lines) vs. the exponent μ, for different values of T_m indicated in the legend. The on-site potential is ϕ^4, $N = 4$, $\Delta_{rel} = 1$ and $k_\mu = 0.2$.